Ru dopant induced high selectivity and stability of ternary RuSnTi electrode toward chlorine evolution reaction

Haiming Gong , Bicheng Zhu , Dianzhi Zhang , Tao Liu , Panyong Kuang [*], Jiaguo Yu [*]

Laboratory of Solar Fuel, Faculty of Materials Science and Chemistry, China University of Geosciences, 68 Jincheng Street, Wuhan 430078, PR China

ARTICLE INFO

ABSTRACT

Chlorine evolution reaction (CER) in chlor-alkali industry is limited by oxygen evolution reaction (OER) due to their common active sites and close standard reaction potentials. Herein, a ternary RuSnTi electrode was synthesized and exhibits a superior CER activity in saturated NaCl solution. Theoretical studies reveal that Ru dopant improves the electrical conductivity of RuSnTi by contributing Ru orbitals to the energy band curves through/near the Fermi level. RuSnTi delivers a current density of 96.6 mA cm^{-2} at potential of 1.15 V (saturated calomel electrode, SCE), much higher than that of the dimensionally stable anode (DSA). Moreover, the inhibitory effect of Sn species on OER endows RuSnTi with a high Cl_2 selectivity of 95.7%. Besides, RuSnTi shows good stability during long-term stability test by stably operating 240 h at 100 mA cm^{-2} in saturated NaCl solution (pH = 7), highlighting the great potential in practical application. This work provides new insights into the development of high-performance Ru-based CER electrodes.

1. Introduction

CER is one of the most widespread and important reactions in industrial production [1–3]. In a typical chlor-alkali process, NaCl reacts with H_2O to produce H_2 and NaOH at the cathode and Cl_2 at the anode, respectively [4]. The cathodic and anodic products could react further to form the chlorate in a diaphragm-free electrolyzer, which has been widely used in the field of chemicals, wastewater treatment, and disinfection. Unfortunately, the side reaction of OER would inevitably occur accompanied by CER due to their commonly used active sites and close standard reaction potentials (U_{CER} = 1.36 V vs. SHE, U_{OER} = 1.23 V vs. RHE) [5–8]. The undesired OER not only reduces the selectivity of Cl_2 but also poses a safety hazard by mixing explosive H_2 with O_2. Therefore, it is a big challenge to improve the Cl_2 selectivity of anode materials.

In past decades, the DSA, which was invented by Dutch scientist H.B. Beer in the late 1960 s, has been the most widely used electrode material in chlor-alkali industry [9,10]. It is an anode made of TiO_2 substrate and mixed metal oxide (MMO) coating layers. The currently used DSA on a large scale is intentionally designed with a Ru:Ti molar ratio of 3:7 according to the patent of Bee67 [11], which exhibits excellent CER performances. However, further improvement of corrosion resistance and Cl_2 selectivity of DSA remains a grand challenge [12]. The development

of low-cost catalysts with excellent activity, selectivity, and stability has become the ultimate goal of scientific researchers [13]. As an alternative, doping with transition metals [14,15], constructing MMO coating layers [16,17], and coupling with single atoms [18] have been proven to be effective strategies for improving the stability and selectivity of anode materials. Among them, doping with transition metals can not only lower the cost of catalysts but also improve the Cl_2 selectivity by adjusting the composition and modulating the structure-activity relationship of the anode. In general, metallic dopants with similar ionic radii to that of Ti^{4+} (such as Sn, Co, Ru, Cd, Mn, Ir, Nb, and Sb) possess a large number of ionic nuclei and strong bonding ability for empty orbitals, which are easier to form a stable solid solution [19–24]. For instance, an Nd-doped IrO_2 electrode prepared by Hu et al. shows a Cl_2 selectivity of 91% and robust stability of over 210 h in 5.0 M NaCl solution (pH = 2) [25]. Lim et al. reported that the Nb-doped ultrafine solid-solution RuO_2/TiO_2 nanoparticle electrode shows a high Faradaic efficiency of 97.3% for Cl_2 generation in 0.6 M NaCl solution, which is far higher than that of the commercial DSA [26]. Further investigations found that Nb doping not only facilitates the electron transfer but also makes Ti atoms diffuse to the lattice of RuO_2 easier to form an ultra-thin TiO_2 protective layer. Shao et al. developed a novel and cost-effective $Ti/Sb-SnO_2/Pb_3O_4$ electrode, which exhibits high activity for Cl_2 evolution and strong anti-corrosion ability [27]. Although a lot of efforts
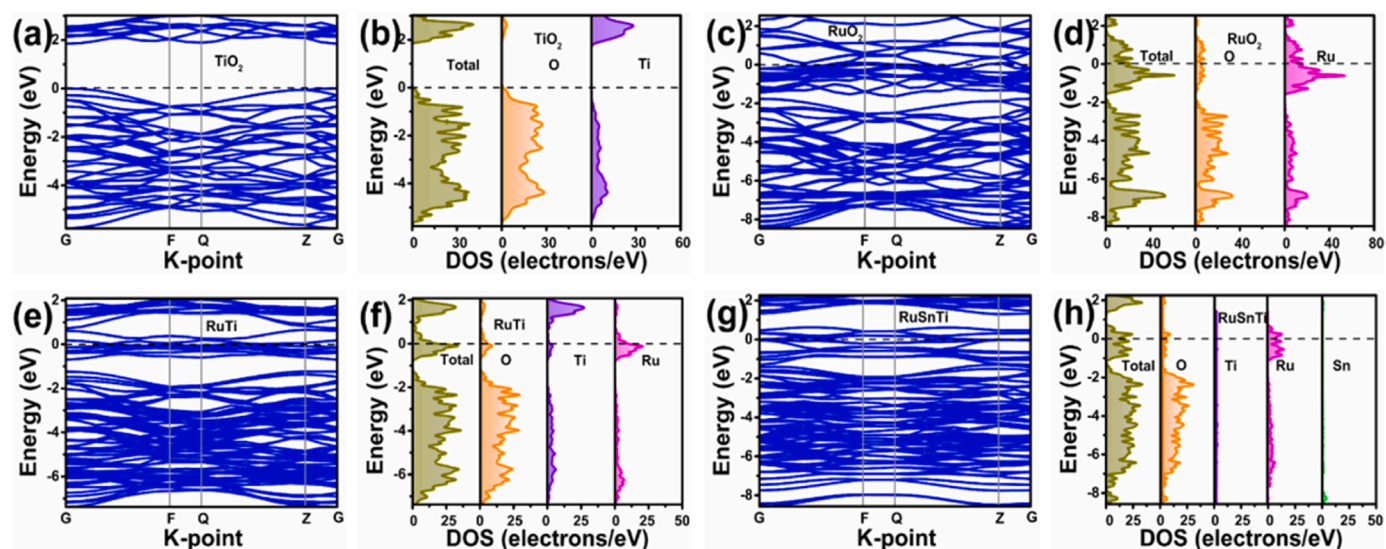
Fig. 1. Band structure and DOS of (a, b) TiO$_2$, (c, d) RuO$_2$, (e, f) RuTi, and (g, h) RuSnTi. Dashed lines represent the Fermi level.

have been made to improve the selectivity and stability of CER, there is still a lot of room for further improvement.

In the case of DSA, both TiO$_2$ and RuO$_2$ are rutile-typed crystals after calcination at a temperature of above 400 °C. According to previous reports, the (110) crystal plane of rutile with the lowest surface energy is conducive to the adsorption of Cl$^-$ anions and the promotion of reaction kinetics [28–30]. However, given the fact that (110) crystal plane of the mainly active RuO$_2$ can catalyze both CER and OER simultaneously, the occupation of active sites by Cl$^-$ or OH$^-$ anions becomes the key to the selectivity of electrocatalyst [31,32]. Therefore, electrocatalytic materials with optimal components and modulated electronic structure are expected to exhibit decreased reaction overpotential and improved durability [33–35]. In this regard, a ternary RuSnTi composite was synthesized and employed as an anode for CER study in this work. Density functional theory (DFT) calculations reveal the indispensability of metallic Ru dopant in increasing the electrical conductivity of RuSnTi, as a result of contributing Ru orbitals to the energy band curves through or near the Fermi level. Further investigations on the adsorption energy of Cl$^-$ and OH$^-$ anions (E_{Cl} and E_{OH}) predict the high Cl$_2$ selectivity of RuSnTi. As expected, RuSnTi exhibits a superior CER activity in saturated NaCl solution (pH = 7), delivering a current density of 96.6 mA cm^{-2} at the potential of 1.15 V (vs. SCE), which is much higher than that of other samples. Moreover, owing to the inhibitory effect of Sn species on O$_2$ evolution, RuSnTi needs a significantly larger potential than other counterparts to achieve the same current density for OER. More importantly, RuSnTi presents the highest selectivity of 95.7% for Cl$_2$ production among all samples and shows good stability with continuous operation for 240 h at 100 mA cm^{-2} in saturated NaCl solution (pH = 7). This work provides constructive insights into the design and fabrication of MMO anodes with excellent CER performances.

2. Experimental details

2.1. Pre-treatment of Ti plate

Firstly, the commercial Ti plate (2 cm × 1 cm × 0.1 cm) was immersed in a mixture solution of acetone and ethanol and ultrasound treated for 30 min. It was then etched with a slightly boiled oxalic acid solution (10 wt%) for 1.5 h to expose a fresh surface. The pre-treated Ti plate was dried naturally and used as a support for the loading of anode materials in the following procedures.

2.2. Preparation of RuSnTi coating solution

Specifically, 50 mg of RuCl$_3$, 32 mg of SnCl$_4$·5 H$_2$O, and 0.062 mL of tetrabutyl titanate (C$_{16}$H$_{36}$O$_4$Ti) (Ru:Sn:Ti = 2:1:2) were dissolved in a mixture solution comprising 0.02 mL of HCl and 0.31 mL of n-butanol, which was then subjected to sufficient ultrasonic treatment to form a homogeneous coating solution. The preparation of RuCoTi and RuSbTi coating solutions was similar to that of RuSnTi, except that 32 mg of SnCl$_4$·5 H$_2$O was replaced by 22 mg of CoCl$_2$·6 H$_2$O and 21 mg of SbCl$_3$, respectively. The molar ratio of Ru:Co:Ti and Ru:Sb:Ti was also maintained at 2:1:2. For comparison, RuTi coating solution was prepared in the absence of SnCl$_4$·5 H$_2$O but with a dosage of 0.15 mL for tetrabutyl titanate.

2.3. Preparation of RuSnTi electrode

A typical thermal decomposition procedure was adopted for RuSnTi electrode preparation. The pre-treated Ti plate was evenly coated by brushing an appropriate amount of coating solution, which was then dried at 150 °C for 5 min. Subsequently, the coated Ti plate was further subjected to 450 °C for 10 min to achieve the thermal decomposition of coating materials. After cooling down to room temperature, the coating and calcination processes were repeated. Finally, the electrode was prepared by repeating the above procedures four times, but with a duration time of 1 h for the last thermal decomposition treatment. Moreover, RuTi, RuCoTi, and RuSbTi were prepared through the same thermal decomposition procedure. Note that a small amount of coating solution will inevitably be lost during the brushing process. For objective comparison, all electrodes were prepared four times. As shown in Table S1, the average loading content of catalysts for RuTi, RuSnTi, RuCoTi, and RuSbTi is calculated to be 5.59, 4.35, 4.95, and 5.16 mg cm^{-2}, respectively.

See Supplementary Material for more details on chemicals, electrochemical measurements, material characterizations, Cl$_2$ selectivity evaluation, and computational details.

3. Results and discussion

3.1. DFT calculations

Compared with TiO$_2$, heteroatom-doped models are geometrically optimized without obvious distortion, confirming the compatibility of Ti, Ru, Sn, Co, and Sb elements (Fig. S1). As shown in Fig. 1a, top of the
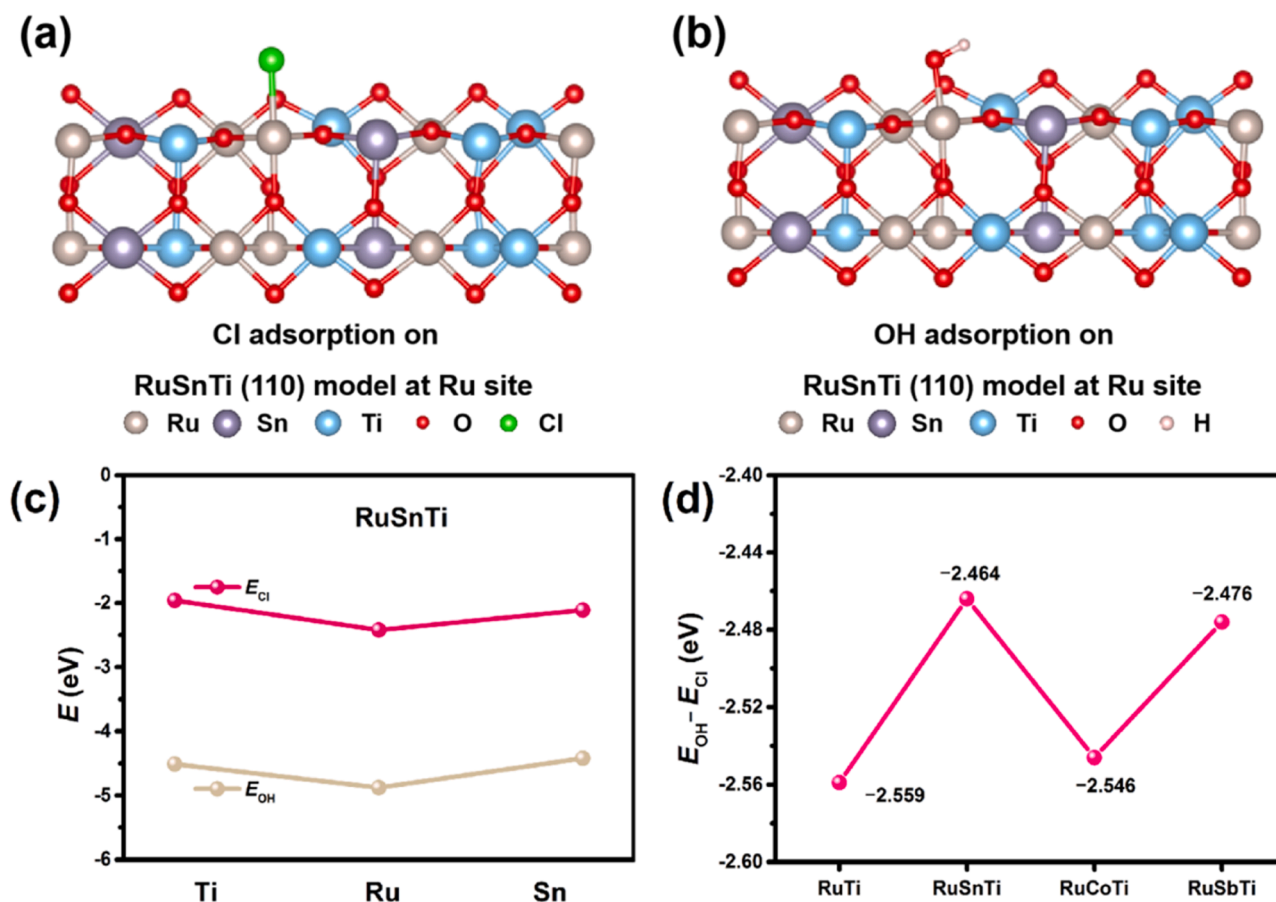
Fig. 2. Side views of (a) Cl^- and (b) OH^- adsorbed RuSnTi (110) model at Ru site. (c) E_{Cl} and E_{OH} of RuSnTi at different sites. (d) $E_{OH} - E_{Cl}$ value of RuTi, RuSnTi, RuCoTi, and RuSbTi.

valance band and bottom of the conduction band of TiO_2 are located at the G-point in k-space, suggesting that TiO_2 is a direct semiconductor with a band gap of 1.86 eV. In contrast, RuO_2 shows a large number of energy band curves through the Fermi level, indicating its metallic property (Fig. 1c). After introducing Ru dopant, the electrical conductivity of binary RuTi is improved compared to that of the bare TiO_2 (Fig. 1e). Similarly, electrical conductivities of the ternary RuSnTi, RuCoTi, and RuSbTi are also improved to different degrees (Fig. 1g and Fig. S2a, c). However, whether the enhanced electrical conductivity of these ternary samples is induced by Ru or other metallic dopants (e.g., Sn, Co, and Sb) needs to be further verified. As can be seen in the density of states (DOS) (Fig. 1b, d, f, h and Fig. S2b, d), unlike TiO_2 with a semiconductor property, energy band curves of all Ru-containing samples through or near the Fermi level are mainly contributed by Ru orbitals, verifying that their improved electrical conductivity is induced by Ru rather than Sn, Co, and Sb dopants. Furthermore, the fundamental reason for improved electrical conductivity is that Ru atom possesses an outer electron structure of $4d^7 5s^1$, which fills the eight-electron shell layers by offering four electrons to two O atoms. Note that there is still an electron-containing band in Ru-containing samples, in which electrons are more easily excited to the conduction band than full electrons. This could reasonably explain the fact that RuO_2 shows both semiconductor and metallic conductor properties and Ru-doped anode materials exhibit superior electrical conductivity [36,37].

It is well known that top metal site usually functions as an active site for reactant adsorption. Therefore, E_{Cl} and E_{OH} of different terminal metal sites were first calculated. As shown in Fig. 2a-c and Fig. S3-S10, Ru sites in RuSnTi, RuCoTi, RuSbTi, and RuTi exhibit both the lowest E_{Cl} and E_{OH} values than Sn, Co, Sb, and Ti sites, suggesting that Ru atom is thermodynamically favorable for the adsorption of Cl^- and OH^- anions.

This result is consistent with the findings that Ru functions as the main active site for CER [38–40]. Moreover, all metal sites show negative E_{Cl} and E_{OH} values, suggesting the exothermic property of the adsorption process [41]. As we all know, the competitive OER needs to be inhibited in CER process, which means that the more positive the E_{OH} value, the inferior the OER performance. Impressively, E_{OH} values of all samples are significantly more negative than E_{Cl}, proving that OER would theoretically occur more easily than CER in this work. However, in the process of chlor-alkali production, OER is not favorable due to the following two aspects. On one hand, a high overpotential is required for OER due to its four-electron process while CER is a facile two-electron process with a kinetic advantage [42]. On the other hand, the concentration of Cl^- anions is much higher than that of the OH^- anion in NaCl solution, making the CER more competitive than OER. Due to the competitive adsorption between Cl^- and OH^- anions, occupation of the Ru active site becomes the main factor affecting the selectivity of CER. Accordingly, the more negative the E_{Cl} and the more positive the E_{OH} on Ru site, the more favorable the CER occurrence and the more improved Cl_2 selectivity. Therefore, the difference between E_{OH} and E_{Cl} (i.e. $E_{OH} - E_{Cl}$) is adopted as a descriptor to predict the Cl_2 selectivity of samples. In other words, the more positive the value of $E_{OH} - E_{Cl}$, the higher the Cl_2 selectivity of sample. As shown in Fig. 2d, the order of Cl_2 selectivity of the samples follows theoretically in a trend of RuSnTi > RuSbTi > RuCoTi > RuTi, which is well verified in the following experimental studies.

3.2. Characterizations

The chemical composition and elemental states of RuSnTi were investigated using X-ray diffraction (XRD) and X-ray photoelectron
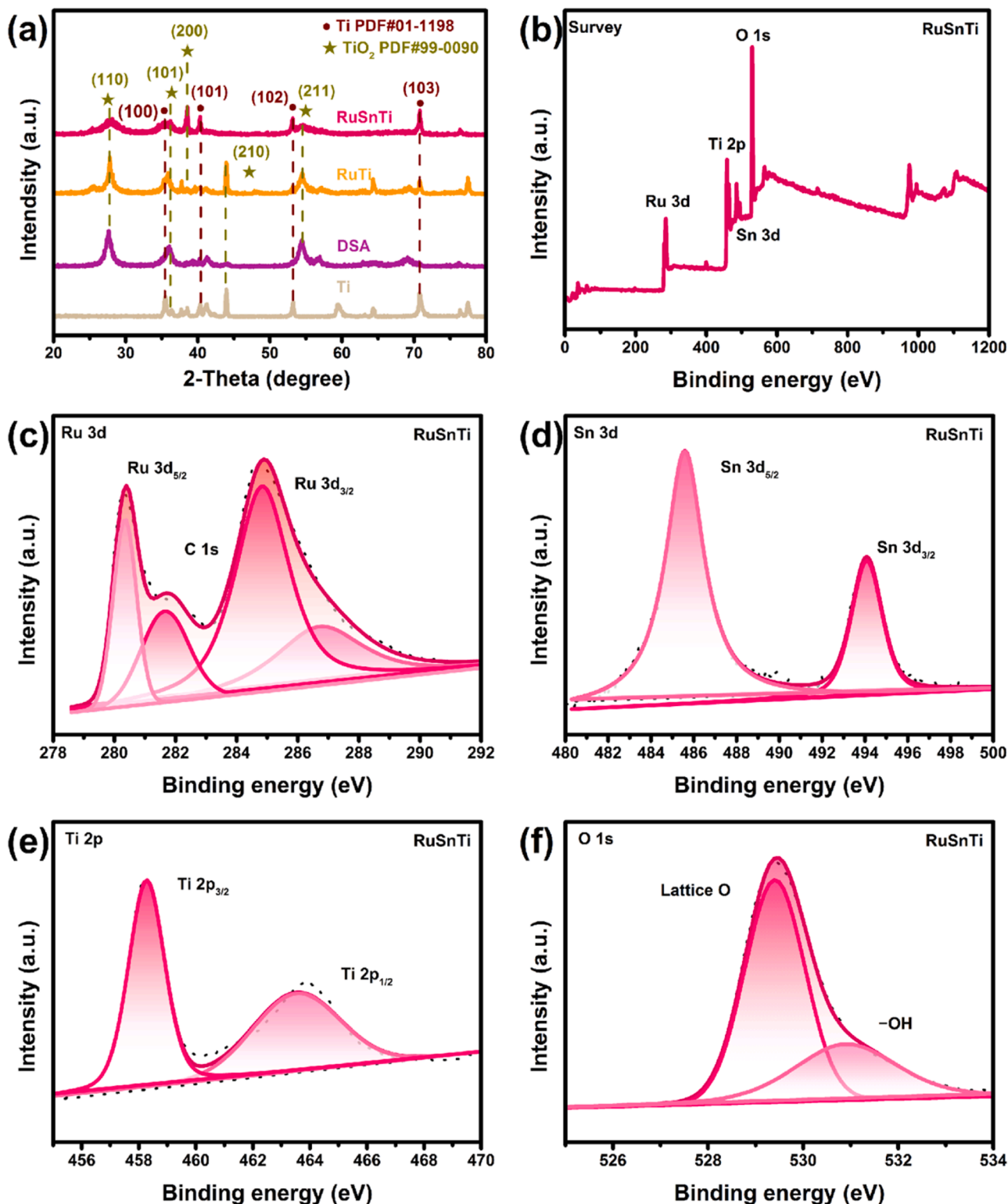
Fig. 3. (a) XRD patterns of RuSnTi, RuTi, DSA, and Ti. (b) XPS survey spectrum, (c) Ru 3d XPS spectrum, (d) Sn 3d XPS spectrum, (e) Ti 2p XPS spectrum, and (f) O 1 s XPS spectrum of the RuSnTi.

spectroscopy (XPS) measurements. As shown in XRD patterns, four diffraction peaks located at 35.3, 40.4, 53.2, and 70.7° can be attributed to the (100), (101), (102), and (103) planes of metal Ti (Fig. 3a). Moreover, three diffraction peaks located at 27.4, 36.0, and 54.3° can be attributed to the (110), (101), and (211) planes of rutile TiO$_2$. Fig. 3b presents the XPS survey spectrum of RuSnTi, displaying the existence of Ru, Sn, Ti, O, and C elements. As shown in Ru 3d XPS spectrum (Fig. 3c),

two peaks centered at 280.3 and 284.9 eV binding energies can be indexed to the Ru 3d$_{3/2}$ and Ru 3d$_{5/2}$ species, respectively [43–45]. Two peaks located at binding energies of 458.3 and 463.6 eV should be ascribed to the Ti 2p$_{3/2}$ and Ti 2p$_{1/2}$ species, respectively (Fig. 3e) [46–48]. The Sn 3d XPS spectrum in Fig. 3d presents two peaks with binding energies of 485.6 and 494.1 eV, which are ascribed to the Sn 3d$_{5/2}$ and Sn 3d$_{3/2}$ species, respectively [49–51]. Moreover, the O 1 s
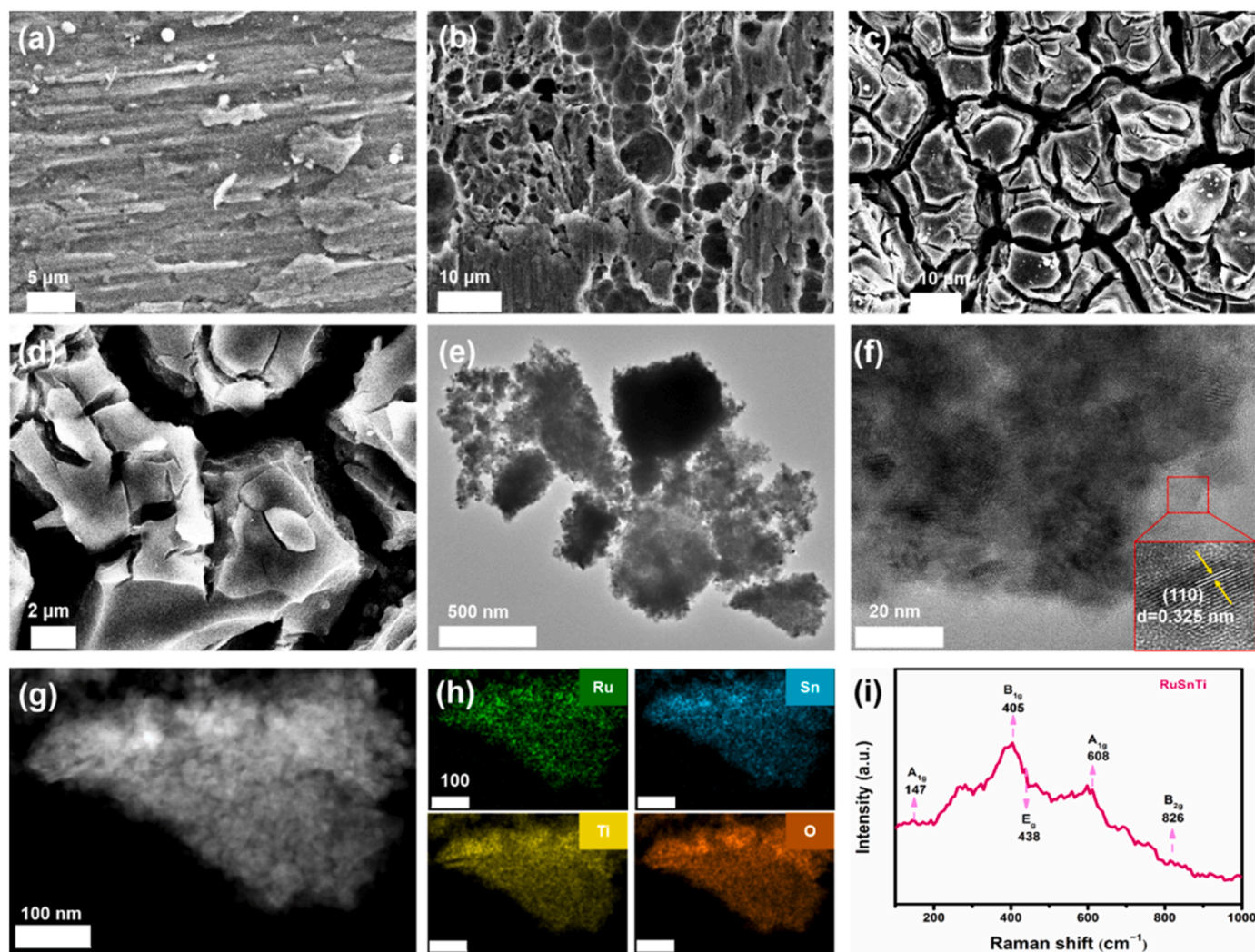
Fig. 4. SEM images of (a) Ti plate, (b) etched Ti plate, and (c-d) RuSnTi. (e) TEM image, (f) HRTEM image, (g-h) EDX elemental mapping images, and (i) Raman spectrum of RuSnTi.

XPS spectrum (Fig. 3f) exhibits two peaks at binding energies of 529.4 and 531.0 eV, which originated from the lattice O and adsorbed H_2O [52,53]. Together with the investigation results of chemical composition and elemental state of other counterparts, RuSnTi, RuCoTi, RuSbTi, and RuTi anode materials have been successfully prepared (Fig. S11-S13). Note that the molar ratios of the metal element in RuSnTi and RuTi are close to the theoretical values while it is not the case in RuCoTi and RuSbTi, which may be attributed to that the Ti plate influences the quantification of metal elements (Table S2).

Compared with bare Ti plate, the chemically etched Ti plate shows a porous and rough surface, which guarantees the impact contact between Ti substrate and coating layer (Fig. 4a-b). Due to the difference in thermal expansion coefficient of Ti substrate and oxide layers, both RuSnTi and other counterpart electrodes show cracked surfaces at different degrees (Fig. 4c-d and Fig. S14-17). It should be emphasized that moderate cracking could expand the active surface area, promote reactant adsorption, and facilitate gaseous product diffusion. However, excessively cracked surfaces would bring the NaCl solution into direct contact with Ti substrate, resulting in passivation and corrosion to the anode. Transmission electron microscopy (TEM) images present the two-dimensional structure of RuSnTi layer, which is composed of oxide nanoparticles (Fig. 4e). High-resolution TEM (HRTEM) image shows a distinct interplanar spacing of 0.325 nm (Fig. 4f), which is assigned to the (110) crystal plane of rutile TiO_2 [54]. Energy dispersive X-ray

(EDX) elemental mapping images reveal the homogeneous distribution of Ru, Sn, Ti, and O elements over RuSnTi layer (Fig. 4g-h). As presented in the Raman spectrum, several peaks located at 147, 405, 438, 608, and 826 cm^{-1} can be ascribed to the A_{1g}, B_{1g}, E_g, A_{1g}, and B_{2g} models of rutile TiO_2, verifying the existence of TiO_2 in ternary RuSnTi after pyrolysis treatment (Fig. 4i). In addition, the rutile phase of TiO_2 is also detected in Raman spectra of other samples (Fig. S18).

3.3. CER performance evaluation

Fig. 5a shows the linear sweep voltammetry (LSV) curves of CER in saturated NaCl solution (pH = 7). RuSnTi delivers a current density of 96.6 mA cm^{-2} at the potential of 1.15 V (vs. SCE), which is significantly higher than that of the RuCoTi (82.7 mA cm^{-2}), RuSbTi (42.0 mA cm^{-2}), RuTi (48.4 mA cm^{-2}), and DSA (3.2 mA cm^{-2}) at the same potential. This result suggests the superior CER activity of RuSnTi. In addition, the CER activity of RuSnTi was evaluated in several NaCl solutions with varied concentrations. As displayed in Fig. S19, the CER activity of RuSnTi increases with increasing the concentration of NaCl solution, suggesting the abundant active sites for Cl_2 evolution and high current conversion efficiency. However, due to the inhibitory effect of Sn species (e.g., SnO_2 with diamagnetic property) on O_2 evolution [8], RuSnTi exhibits a stronger inhibition ability for OER than other samples in 0.5 M H_2SO_4 solution. As displayed in Fig. 5b, unlike the LSV curve
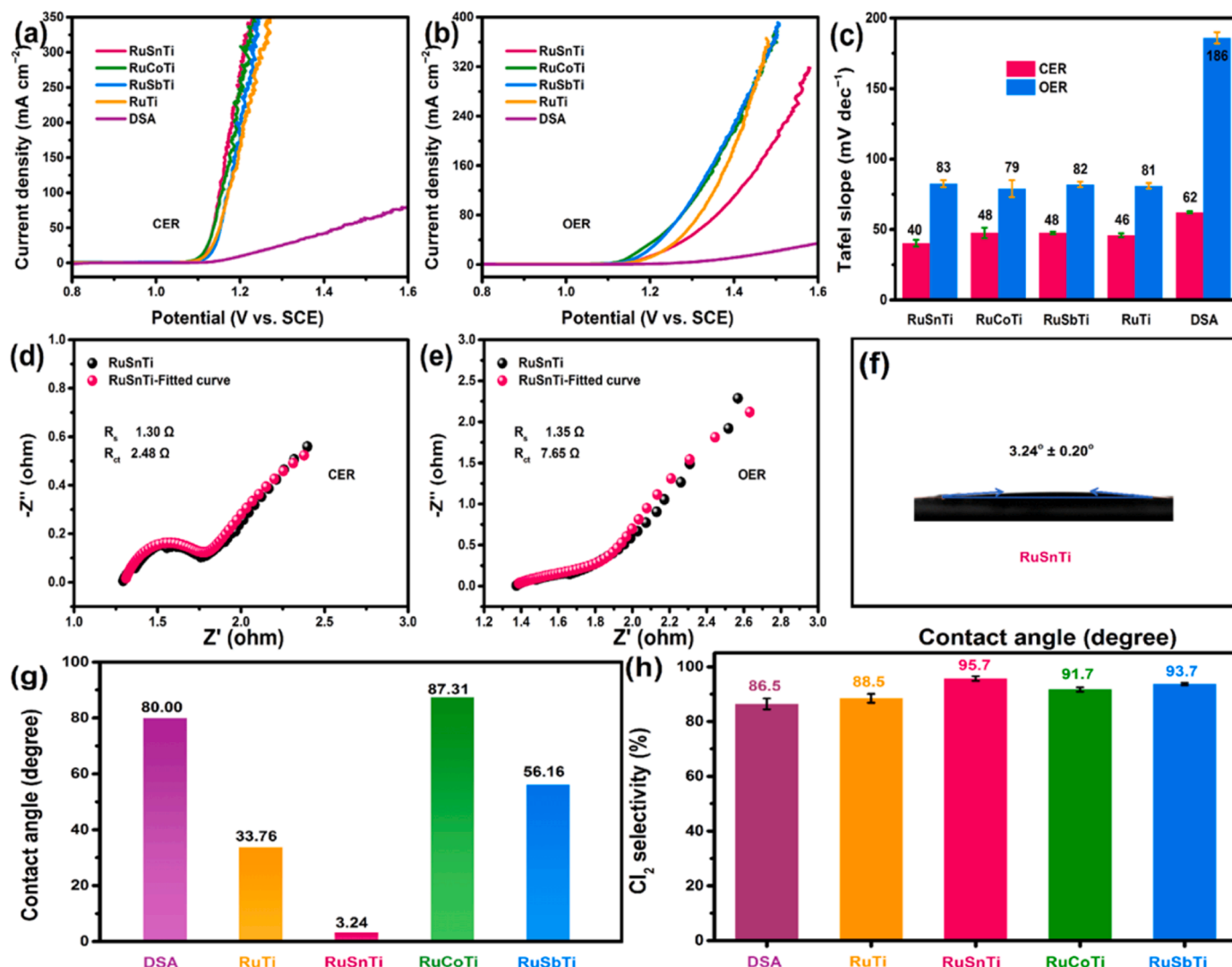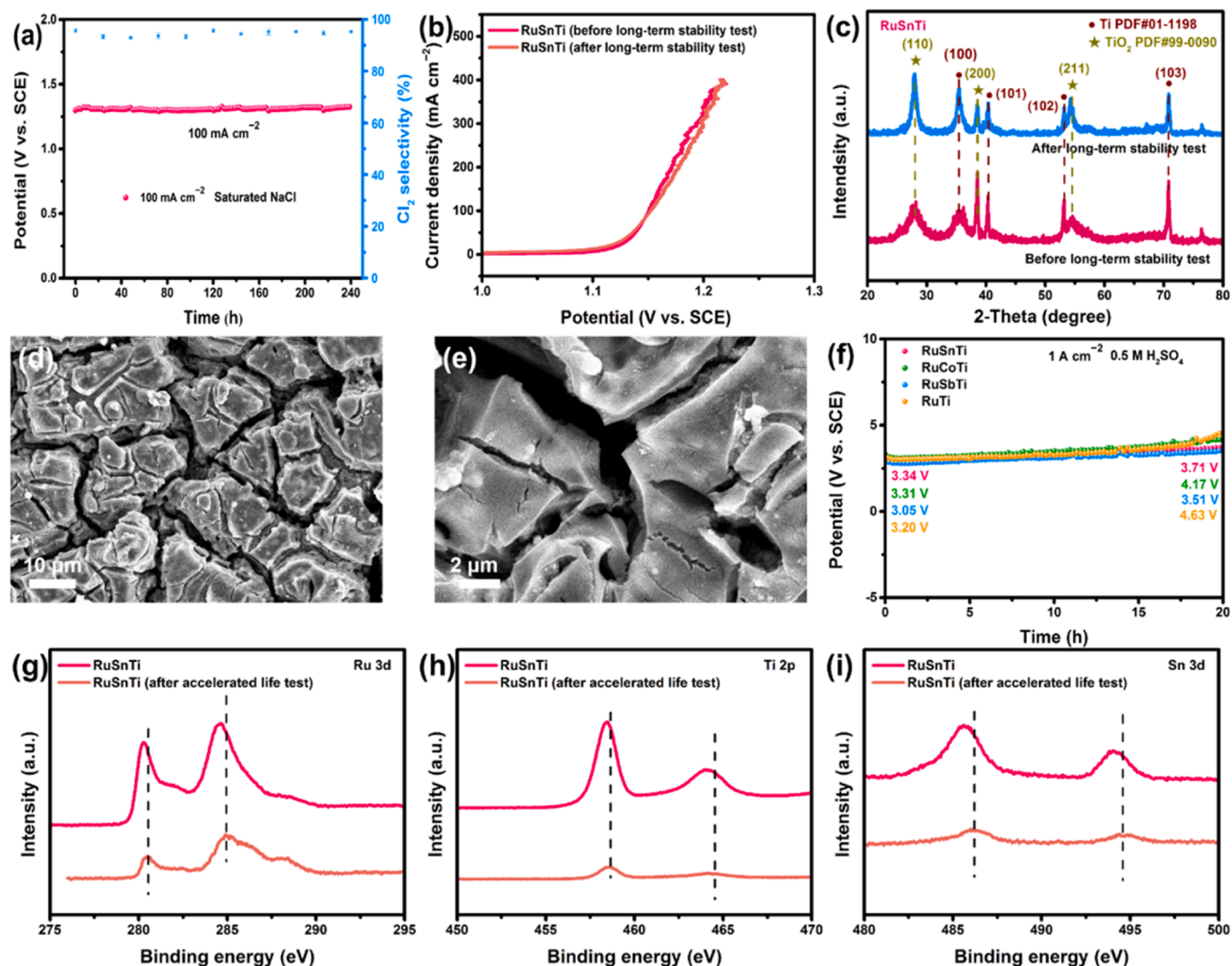
Fig. 5. (a) CER LSV curves (saturated NaCl solution (pH = 7)), (b) OER LSV curves (0.5 M H_2SO_4 solution), and (c) corresponding Tafel slopes of RuSnTi, RuCoTi, RuSbTi, RuTi, and DSA. (d, e) CER and OER EIS plots of RuSnTi. (f, g) Contact angle and (h) Cl_2 selectivity of RuSnTi, RuCoTi, RuSbTi, RuTi, and DSA.

for CER, the potential required for RuSnTi to achieve the same current density is significantly larger than that of other samples. For instance, RuSnTi needs a large potential of 1.11 V to reach a current density of 100 mA cm^{-2}, much higher than that of the RuCoTi (0.99 V), RuSbTi (1.07 V), and RuTi (1.09 V). In addition to 0.5 M H_2SO_4 solution, RuSnTi also shows poor OER activity in other Cl-free solutions including Na_2SO_4, $NaNO_3$, and H_2O (Fig. S20). Note that although DSA shows extremely inhibited OER behavior, the low current density for CER reveals its unsatisfactory Cl_2 selectivity. Electrochemical active surface area (ECSA) measurements show that the number of active sites in RuSnTi is an order of magnitude larger than that of DSA (Fig. S21). Note that RuSnTi exhibits a lower ECSA value than RuCoTi and RuSbTi, which can be ascribed to the fact that Co and Sb can also serve as active sites for OER in addition to Ru [55–57]. Therefore, it is reasonable that RuSnTi shows higher CER activity than RuCoTi and RuSbTi whereas inferior OER activity to them. Tafel slope is widely used to elucidate the reaction kinetics and underlying mechanism. As shown in Fig. 5c, all samples show lower Tafel slopes in saturated NaCl solution (pH = 7) than in 0.5 M H_2SO_4 solution, suggesting their favorable reaction kinetics of CER. RuSnTi exhibits a Tafel slope of 40 mV dec^{-1} in saturated NaCl solution, indicating the Volmer-Heyrovsky mechanism with two electrons transfer [10]. Cl^- anion is initially adsorbed on the active site to form an adsorbed Cl atom (Volmer step: $M^* + 2Cl^- \rightarrow M^*-Cl + e^- +$

Cl^-) [58], which then combines with another Cl^- anion to generate a Cl_2 molecule (Heyrovsky step: $M^*-Cl + e^- + Cl^- \rightarrow M^* + Cl_2 + 2e^-$) [20]. In addition, Tafel slopes of all as-prepared MMO in saturated NaCl solution are much lower than those of DSA, demonstrating that these anode materials have stronger capabilities of exhibiting faster reaction kinetics and obtaining larger current density increments for CER [58, 59].

Electrochemical impedance spectroscopy (EIS) measurements were further conducted to reveal the superior electron transfer ability of RuSnTi [60]. Fig. 5d and Fig. S22 show the EIS plots of CER, in which RuSnTi presents the smallest charge transfer resistance (R_{ct} = 2.48 Ω) in low-frequency region in comparison with other samples, confirming the reduced electron transfer resistance and promoted mass transfer ability at electrode/electrolyte interface. Moreover, RuSnTi exhibits a quite smaller R_{ct} value (7.65 Ω) than DSA in the case of OER (Fig. 5e and Fig. S23), suggesting its significantly lower charge transfer resistance, which agrees well with the observations that RuSnTi possesses higher OER activity than DSA. However, the OER activity of RuSnTi is still suppressed due to the previously mentioned inhibitory effect of Sn species on O_2 evolution. In addition, RuSnTi shows the smallest contact angle among all samples for saturated NaCl solution, demonstrating its super-hydrophilic property which should be one of the important reasons for the excellent mass transfer ability (Fig. 5f-g and Fig. S24). Cl_2

Fig. 6. (a) Long-term stability test of RuSnTi at 100 mA cm^{-2} in saturated NaCl solution (pH = 7). (b) CER LSV curves and (c) XRD patterns of RuSnTi before and after long-term stability test. (d, e) SEM images of RuSnTi after long-term stability test. (f) Accelerated life test of RuSnTi, RuCoTi, RuSbTi, and RuTi at 1 A cm^{-2} in 0.5 M H$_2$SO$_4$ solution. (g) Ru 3d, (h) Ti 2p, and (i) Sn 3d XPS spectrum of RuSnTi before and after accelerated life test.

selectivity is one of the most important and intuitive parameters to evaluate CER performance. As shown in Fig. 5h, RuSnTi exhibits the highest Cl$_2$ selectivity of 95.7% among all samples, suggesting its extraordinary CER activity with high electron utilization efficiency for Cl$_2$ generation. The trend of Cl$_2$ selectivity is consistent with the above theoretical investigations that RuSnTi possesses the most positive value of $E_{OH} - E_{Cl}$ among all samples. The highest Cl$_2$ selectivity of RuSnTi unambiguously confirms the strong adsorption ability for Cl$^-$ anion and suggests the greatly suppressed OER behavior.

3.4. Stability evaluation

Together with activity and selectivity, stability is also an important parameter for evaluating the CER performance. Therefore, long-term stability of RuSnTi was examined through a chronopotentiometry test at a fixed current density of 100 mA cm^{-2} in saturated NaCl solution (pH = 7). As shown in Fig. 6a, the applied potential remains almost unchanged to retain the current density of 100 mA cm^{-2} after a consecutive operation for 240 h, and the Cl$_2$ selectivity is maintained as high as the initial one at the same time. The Cl$_2$ selectivity and stability of RuSnTi are comparable to many previously reported CER catalysts (Table S3). Furthermore, LSV curves, EIS plots, XRD patterns, and SEM

images prove the well-maintained CER activity and microstructures of RuSnTi after the long-term stability test (Fig. 6b-e and Fig. S25). These results ambiguously reveal the high stability of RuSnTi. In addition to the neutral saturated NaCl solution, RuSnTi also possesses extraordinary stability in acidic saturated NaCl solution at a high current density of 250 mA cm^{-2} (Fig. S26). The superior stability in different conditions strongly suggests the potential application of RuSnTi in complex environments. Accelerated life test is another method to assess the stability of catalysts. Fig. 6f displays the accelerated life test of RuSnTi under a harsh condition (1 A cm^{-2}, 0.5 M H$_2$SO$_4$). Compared to other samples, the relatively higher potential of RuSnTi (3.34 V) at the beginning reveals its poor OER activity. This result is consistent with the above observation that the OER activity of RuSnTi is inferior to other samples (Fig. 5b). More importantly, RuSnTi shows the smallest increment in applied potential after a consecutive test for 20 h, indicating that Sn doping has a positive effect on the inhibition of OER and the poor OER activity is quite conducive to the maintenance of stability. Note that further investigations found that RuSnTi suffered from slight oxidation and dissolution during the accelerated life test. The concentration of Ru, Sn, and Ti elements in electrolytes increases after the accelerated life test, and the loss of active Ru species causes RuSnTi to exhibit decreased activity and increased mass transfer resistance (Table S4 and Fig. S27).

According to the precursor utilization, loaded amount of RuSnTi on Ti plate, and metal concentration variation in electrolyte, the metal loss rate of Ru, Sn, and Ti was basically calculated to be 10.0, 3.8, and 12.0%, respectively. XPS measurements show the positive shift of binding energy for Ru, Ti, and Sn elements after the accelerated life test (Fig. 6g-i), which can be reasonably ascribed to the oxidation of RuSnTi under highly oxidative (OER) conditions [61].

4. Conclusion

In summary, this work constructed a ternary RuSnTi electrode and established it as a highly active and selective anode for CER application. Due to the cracked structure and Ru doping, RuSnTi shows a superior CER activity in saturated NaCl solution, delivering a current density of 96.6 mA cm^{-2} at the potential of 1.15 V (vs. SCE), much higher than that of DSA at the same potential. DFT calculations show that Ru dopant improves the electrical conductivity of RuSnTi, by contributing Ru orbitals to the energy band curves through or near the Fermi level. Tafel slope and Nyquist plots further demonstrate the superior reaction kinetics and charge transfer ability of RuSnTi. More importantly, due to the inhibitory effect of Sn species on OER behavior, RuSnTi presents the highest Cl$_2$ selectivity of 95.7% compared to RuCoTi, SuSbTi, RuTi, and DAS. In addition, RuSnTi exhibits excellent long-term stability with continuous operation for 240 h at 100 mA cm^{-2} in saturated NaCl solution (pH = 7), indicating its potential in practical application. This work offers valuable insights into the exploration of highly efficient Ru-containing anodes for CER application.

CRediT authorship contribution statement

Bicheng Zhu: Data curation. **Haiming Gong:** Writing – original draft, Methodology, Formal analysis, Data curation, Conceptualization. **Jiaguo yu:** Writing – review & editing, Supervision, Conceptualization. **Panyong Kuang:** Writing – review & editing, Supervision, Conceptualization. **Tao Liu:** Software, Funding acquisition, Data curation. **Dianzhi Zhang:** Writing – original draft, Methodology, Formal analysis, Data curation, Conceptualization.

Declaration of Competing Interest

The authors declare that they have no known competing financial interests or personal relationships that could have appeared to influence the work reported in this paper.

Data availability

Data will be made available on request.

Acknowledgments

Appendix A. Supporting information

Supplementary data associated with this article can be found in the online version at doi:10.1016/j.apcatb.2024.123892.

References

[1] H. Lim, D. Cho, J. Park, S. Ji, Y. Ahn, J. Kim, C. Lee, Rational design of dimensionally stable anodes for active chlorine generation, ACS Catal. 11 (2021) 12423–12432.
[2] K. Exner, Beyond dimensionally stable anodes: single-atom catalysts with superior chlorine selectivity, ChemElectroChem 7 (2020) 1528–1530.
[3] B. Cui, Y. Shi, G. Li, Ya Chen, W. Chen, Y. Deng, W. Hu, Challenges and opportunities for seawater electrolysis: A mini-review on advanced materials in chlorine-involved electrochemistry, Acta Phys. −Chim. Sin. 38 (2022) 2106010.
[4] H. Over, Atomic scale insights into electrochemical versus gas phase oxidation of HCl over RuO$_2$-based catalysts: a comparative review, Electrochim. Acta 93 (2013) 314–333.
[5] R. Karlsson, A. Cornell, Selectivity between oxygen and chlorine evolution in the chlor-alkali and chlorate processes, Chem. Rev. 116 (2016) 2982–3028.
[6] J. Vos, T. Wezendonk, A. Jeremiasse, M. Koper, MnO$_x$/IrO$_x$ as selective oxygen evolution electrocatalyst in acidic chloride solution, J. Am. Chem. Soc. 140 (2018) 10270–10281.
[7] M. Xiao, Q. Wu, R. Ku, L. Zhou, C. Long, J. Liang, A. Mavrič, L. Li, J. Zhu, M. Valant, J. Li, Z. Zeng, C. Cui, Self-adaptive amorphous CoO$_x$Cl$_y$ electrocatalyst for sustainable chlorine evolution in acidic brine, Nat. Commun. 14 (2023) 5356.
[8] D. Zhang, F. Xie, H. Gong, T. Liu, P. Kuang, J. Yu, Enhancing Ru−Cl interaction via orbital hybridization effect in Ru$_{0.4}$Sn$_{0.3}$Ti$_{0.3}$ electrode for efficient chlorine evolution, J. Colloid Interface Sci. 658 (2024) 127–136.
[9] M. Jiang, H. Wang, Y. Li, H. Zhang, G. Zhang, Z. Lu, X. Sun, L. Jiang, Superaerophobic RuO$_2$-based nanostructured electrode for high-performance chlorine evolution reaction, Small 13 (2017) 1602240.
[10] Y. Wang, Y. Xue, C. Zhang, Rational surface and interfacial engineering of IrO$_2$/TiO$_2$ nanosheet arrays toward high-performance chlorine evolution electrocatalysis and practical environmental remediation, Small 17 (2021) 2006587.
[11] Beer, H.B. Method of making an electrode having a coating containing a platinum metal oxide thereon, US. US3840443A.
[12] A. Zeradjanin, F. Mantia, J. Masa, W. Schuhmann, Utilization of the catalyst layer of dimensionally stable anodes-interplay of morphology and active surface area, Electrochim. Acta 82 (2012) 408–414.
[13] L. Zhang, J. Zhu, X. Li, S. Mu, F. Verpoort, J. Xue, Z. Kou, J. Wang, Nurturing the marriages of single atoms with atomic clusters and nanoparticles for better heterogeneous electrocatalysis, Interdiscip. Mater. 1 (2022) 51–87.
[14] V. Petrykin, K. Macounova, J. Franc, O. Shlyakhtin, M. Klementova, S. Mukerjee, P. Krtil, Zn-doped RuO$_2$ electrocatalyts for selective oxygen evolution: relationship between local structure and electrocatalytic behavior in chloride containing media, Chem. Mater. 23 (2011) 200–207.
[15] H. Cao, D. Lu, J. Lin, Q. Ye, J. Wu, G. Zheng, Novel Sb-doped ruthenium oxide electrode with ordered nanotube structure and its electrocatalytic activity toward chlorine evolution, Electrochim. Acta 91 (2013) 234–239.
[16] J. Vos, Z. Liu, F. Speck, N. Perini, W. Fu, S. Cherevko, M. Koper, Selectivity trends between oxygen evolution and chlorine evolution on iridium-based double perovskites in acidic media, ACS Catal. 9 (2019) 8561–8574.
[17] R. Karlsson, H. Hansen, T. Bligaard, A. Cornell, L. Pettersson, Ti atoms in Ru$_{0.3}$Ti$_{0.7}$O$_2$ mixed oxides form active and selective sites for electrochemical chlorine evolution, Electrochim. Acta 146 (2014) 733–740.
[18] T. Lim, G. Jung, J. Kim, S. Park, J. Park, Y. Kim, S. Kang, H. Jeong, S. Kwak, S. Joo, Atomically dispersed Pt–N$_4$ sites as efficient and selective electrocatalysts for the chlorine evolution reaction, Nat. Commun. 11 (2020) 412.
[19] S. Evdokimov, Electrochemical and corrosion behavior of electrode materials based on compositions of ruthenium dioxide and base-metal oxides, Russ. J. Electrochem. 38 (2002) 583–588.
[20] V. Trieu, B. Schley, H. Natter, J. Kintrup, A. Bulan, R. Hempelmann, RuO$_2$-based anodes with tailored surface morphology for improved chlorine electro-activity, Electrochim. Acta 78 (2012) 188–194.
[21] J. Ribeiro, P. Alves, A. Andrade, Effect of the preparation methodology on some physical and electrochemical properties of Ti/Ir$_x$Sn$_{(1−x)}$O$_2$ materials, J. Mater. Sci. 42 (2007) 9293–9299.
[22] M. Santana, L. Faria, Oxygen and chlorine evolution on RuO$_2$+TiO$_2$+CeO$_2$+Nb$_2$O$_5$ mixed oxide electrodes, Electrochim. Acta 51 (2006) 3578–3585.
[23] K. Meaney, S. Omanovic, Sn$_{0.86}$-Sb$_{0.03}$-Mn$_{0.10}$-Pt$_{0.01}$-oxide/Ti anode for the electro-oxidation of aqueous organic wastes, Mater. Chem. Phys. 105 (2007) 143–147.
[24] D. Cestarolli, A. Andrade, Electrochemical and morphological properties of Ti/RuO$_2$Pb$_{(0.7−x)}$Ti$_x$O$_2$-coated electrodes, Electrochim. Acta 48 (2003) 4137–4142.
[25] J. Hu, H. Xu, X. Feng, L. Lei, Y. He, X. Zhang, Neodymium-doped IrO$_2$ electrocatalysts supported on titanium plates for enhanced chlorine evolution reaction performance, ChemElectroChem 8 (2021) 1204–1210.
[26] H. Lim, D. Cho, J. Park, S. Ji, Y. Ahn, J. Kim, C. Lee, Rational design of dimensionally stable anodes for active chlorine generation, ACS Catal. 11 (2021) 12423–12432.
[27] D. Shao, W. Yan, L. Cao, X. Li, H. Xu, High-performance Ti/Sb−SnO$_2$/Pb$_3$O$_4$ electrodes for chlorine evolution: preparation and characteristics, J. Hazard. Mater. 267 (2014) 238–244.
[28] Q. Huang, L. Gao, A simple route for the synthesis of rutile TiO$_2$ nanorods, Chem. Lett. 32 (2003) 638–639.
[29] E. Hosono, S. Fujihara, K. Kakiuchi, H. Imai, Growth of submicrometer-scale rectangular parallelepiped rutile TiO$_2$ films in aqueous TiCl$_3$ solutions under hydrothermal conditions, J. Am. Chem. Soc. 126 (2004) 7790–7791.
[30] J. Rossmeisl, Z. Qu, H. Zhu, G. Kroes, J. Norskov, Electrolysis of water on oxide surfaces, J. Electroanal. Chem. 607 (2007) 83–89.

[31] H. Hansen, I. Man, F. Studt, F. Abild-Pedersen, T. Bligaard, J. Rossmeisl, Electrochemical chlorine evolution at rutile oxide (110) surfaces, Phys. Chem. Chem. Phys. 12 (2010) 283–290.

[32] L. Krishtalik, Kinetics and mechanism of anodic chlorine and oxygen evolution reactions on transition metal oxide electrodes, Electrochim. Acta 26 (1981) 329–337.

[33] T. Lassali, S. Castro, J. Boodts, Structural morphological and surface properties as a function of composition of Ru+Ti+Pt mixed-oxided electrodes, Electrochim. Acta 43 (1998) 2515–2525.

[34] P. Kuang, Y. Wang, B. Zhu, F. Xia, C. Tung, J. Wu, H. Chen, J. Yu, Pt single atoms supported on N-doped mesoporous hollow carbon spheres with enhanced electrocatalytic H_2-evolution activity, Adv. Mater. 33 (2021) 2008599.

[35] P. Kuang, Z. Ni, B. Zhu, Y. Lin, J. Yu, Modulating the d-band center enables ultrafine Pt_3Fe alloy nanoparticles for pH-universal hydrogen evolution reaction, Adv. Mater. 35 (2023) 2303030.

[36] H. Over, Surface chemistry of ruthenium dioxide in heterogeneous catalysis and electrocatalysis: from fundamental to applied research, Chem. Rev. 112 (2012) 3356–3426.

[37] M. García-Mota, A. Vojvodic, F. Abild-Pedersen, J. Nørskov, Electronic origin of the surface reactivity of transition metal doped TiO_2 (110), J. Phys. Chem. C. 117 (2013) 460–465.

[38] S. Trasatti, Electrocatalysis: understanding the success of DSA, Electrochim. Acta 45 (2000) 2377–2385.

[39] L. Näslund, C. Sánchez-Sánchez, A. Ingason, J. Bäckström, E. Herrero, J. Rosen, S. Holmin, The role of TiO_2 doping on RuO_2-coated electrodes for the water oxidation reaction, J. Phys. Chem. C. 117 (2013) 6126–6135.

[40] D. Kuo, H. Paik, J. Nelson, K. Shen, D. Schlom, J. Suntivich, Chlorine evolution reaction electrocatalysis on RuO_2 (110) and IrO_2 (110) grown using molecular-beam epitaxy, J. Chem. Phys. 150 (2019) 041726.

[41] Q. Xu, J. Yu, J. Zhang, J. Zhang, G. Liu, Cubic anatase TiO_2 nanocrystals with enhanced photocatalytic CO_2 reduction activity, Chem. Commun. 51 (2015) 7950–7953.

[42] Y. Kuang, M. Kenney, Y. Meng, W. Hung, Y. Liu, J. Huang, R. Prasanna, P. Li, Y. Li, L. Wang, M. Lin, M. McGehee, X. Sun, H. Dai, Solar-driven, highly sustained splitting of seawater into hydrogen and oxygen fuels, Proc. Natl. Acad. Sci. USA 116 (2019) 6624–6629.

[43] S. Jeon, J. Jeong, H. Yoo, H. Yu, B. Kim, M. Kim, RuO_2 nanorods on electrospun carbon nanofibers for supercapacitors, ACS Appl. Nano Mater. 3 (2020) 3847–3858.

[44] S. Cao, F. Ye, N. Zhang, Y. Guo, Y. Guo, L. Wang, S. Dai, W. Zhan, Synergistic effect of bimetallic $RuPt/TiO_2$ catalyst in methane combustion, Rare Met. 42 (2023) 165–175.

[45] Z. Qin, Y. Chen, X. Wang, N. Wei, X. Liu, H. Chen, Y. Miao, Y. Zhao, Zwitterion-functionalized SnO_2 substrate induced sequential deposition of black-phase $FAPbI_3$ with rearranged PbI_2 residue, Adv. Mater. 34 (2022) 2203143.

[46] T. Nguyen-Phan, S. Luo, D. Vovchok, J. Llorca, J. Graciani, J. Sanz, S. Sallis, W. Xu, J. Bai, L. Piper, D. Polyansky, E. Fujita, S. Senanayake, D. Stacchiola, J. Rodriguez, Visible light-driven H_2 production over highly dispersed ruthenia on rutile TiO_2 nanorods, ACS Catal. 6 (2016) 407–417.

[47] Y. Yang, B. Zhu, L. Wang, B. Cheng, L. Zhang, J. Yu, In-situ grown N, S co-doped graphene on TiO_2 fiber for artificial photosynthesis of H_2O_2 and mechanism study, Appl. Catal. B: Environ. 317 (2022) 121788.

[48] H. Zhao, Y. Qi, K. Liang, W. Zhu, H. Wu, J. Li, Y. Ren, Phosphorus-doping and oxygen vacancy endowing anatase TiO_2 with excellent sodium storage performance, Rare Met. 41 (2022) 1284–1293.

[49] L. Wang, Q. Zhao, Z. Wang, Y. Wu, X. Ma, Y. Zhu, C. Cao, Cobalt-doping SnS_2 nanosheets towards high-performance anodes for sodium ion batteries, Nanoscale 12 (2020) 248–255.

[50] J. Wu, C. Zhen, G. Liu, Photo-assisted Cl doping of SnO_2 electron transport layer for hysteresis-less perovskite solar cells with enhanced efficiency, Rare Met. 41 (2022) 361–367.

[51] S. Sun, H. Jiang, Z. Chen, Q. Chen, M. Ma, L. Zhen, B. Song, C. Xu, Bifunctional WC-supported RuO_2 nanoparticles for robust water splitting in acidic media, Angew. Chem. Int. Ed. 61 (2022) 202202519.

[52] Y. Yang, B. Cheng, J. Yu, L. Wang, W. Ho, TiO_2/In_2S_3 S-scheme photocatalyst with enhanced H_2O_2-production activity, Nano Res. 16 (2023) 4506–4514.

[53] P. Kuang, M. He, B. Zhu, J. Yu, K. Fan, M. Jaroniec, 0D/2D NiS_2/V-MXene composite for electrocatalytic H_2 evolution, J. Catal. 375 (2019) 8–20.

[54] L. Yu, Y. Shao, D. Li, Direct combination of hydrogen evolution from water and methane conversion in a photocatalytic system over Pt/TiO_2, Appl. Catal. B: Environ. 204 (2017) 216–223.

[55] A. Babaei, M. Rezaei, Development of a highly stable and active non-precious anode electrocatalyst for oxygen evolution reaction in acidic medium based on nickel and cobalt-containing antimony oxide, J. Electroanal. Chem. 935 (2023) 117319.

[56] H. Koppisetti, S. Ganguli, S. Ghosh, V. Mahalingam, Rejuvenating the geometric electrocatalytic OER performance of crystalline Co_3O_4 by microstructure engineering with sulfate, Chem. Asian J. 16 (2021) 988–998.

[57] L. Qi, M. Wang, X. Li, Graphene-induced growth of Co_3O_4 nanoplates with modulable oxygen vacancies for improved OER properties, CrystEngComm 23 (2021) 7928–7931.

[58] J. Vos, A. Venugopal, W. Smith, M. Koper, Competition and selectivity during parallel evolution of bromine, chlorine and oxygen on IrO_x electrodes, J. Catal. 389 (2020) 99–110.

[59] L. Li, P. Wang, Q. Shao, X. Huang, Metallic nanostructures with low dimensionality for electrochemical water splitting, Chem. Soc. Rev. 49 (2020) 3072–3106.

[60] Y. Wang, B. Zhu, B. Cheng, W. Macyk, P. Kuang, J. Yu, Hollow carbon sphere-supported Pt/CoO_x hybrid with excellent hydrogen evolution activity and stability in acidic environment, Appl. Catal. B: Environ. 314 (2022) 121503.

[61] Z. Deng, S. Xu, C. Liu, X. Zhang, M. Li, Z. Zhao, Stability of dimensionally stable anode for chlorine evolution reaction, Nano Res. 17 (2024) 949–959.